

The Nonlinear Talbot Effect of Rogue Waves

Yiqi Zhang^{1,*}, Milivoj R. Belić^{2,†}, Huaibin Zheng¹, Haixia Chen¹, Changbiao Li¹, Jianping Song¹, and Yanpeng Zhang^{1‡}
¹Key Laboratory for Physical Electronics and Devices of the Ministry of Education & Shaanxi Key Lab of Information Photonic Technique, Xi'an Jiaotong University, Xi'an 710049, China

²Science Program, Texas A&M University at Qatar, P.O. Box 23874 Doha, Qatar

(Dated: June 14, 2018)

Akhmediev and Kuznetsov-Ma breathers are rogue wave solutions of the nonlinear Schrödinger equation (NLSE). Talbot effect (TE) is an image recurrence phenomenon in the diffraction of light waves. We report the nonlinear TE of rogue waves in a cubic medium. It is different from the linear TE, in that the wave propagates in a NL medium and is an eigenmode of NLSE. Periodic rogue waves impinging on a NL medium exhibit recurrent behavior, but only at the TE length and at the half-TE length with a π -phase shift; the fractional TE is absent. The NL TE is the result of the NL interference of the lobes of rogue wave breathers. This interaction is related to the transverse period and intensity of breathers, in that the bigger the period and the higher the intensity, the shorter the TE length.

PACS numbers: 42.30.Wb, 42.65.Hw, 42.65.Jx, 42.65.Tg, 42.81.Dp

Introduction.—Talbot effect (TE) is a recurrent self-imaging phenomenon in the near-field diffraction of plane waves from a grating, first observed in 1836 by H. F. Talbot [1] and theoretically explained in 1881 by Lord Rayleigh [2]. In the past decade TE has attracted a lot of attention, owing to its potential applications in image preprocessing and synthesis, photolithography, spectrometry, optical computing, and elsewhere. Until now, TE has been reported in, but not confined to, the following areas of physics: atomic optics [3], quantum optics [4], waveguide arrays [5], photonic lattices [6], Bose-Einstein condensates [7], X-ray imaging [8], and in the interferometer for C₇₀ fullerene molecules [9]. Very recently, a nonlinear (NL) TE was reported in Ref. [10]. It is different from the NL TE reported here, in that it refers to the linear TE from a NL wave. For a more thorough introduction, one may consult the recent review paper [11]. However, all these investigations do not report TE in NL media, not even the so-called NL TE in Refs. [10, 11]. This task is accomplished in this Letter.

As a phenomenon first spotted in oceans, the rogue wave is now commonly observed in NL optics [12, 13]. Today, it is accepted that rogue waves are adequately described by the NLSE; they come in a variety of forms that include Peregrine solitons [14], Kuznetsov-Ma breathers (KMBs) [15], Akhmediev breathers (ABs) [16], and higher-order rogue wave solutions [17]. To observe TE it is necessary that the diffracting pattern is periodic in the transverse direction. Hence, we study the TE of rogue wave breathers that are periodically modulated in the transverse coordinate. However, different from the linear TE, the diffracting patterns propagate in the NL medium and are the eigenmodes of NLSE.

Again, the nonlinear TE reported in this Letter is in stark contrast to the linear one, which needs real gratings or periodic diffracting structures, forms in linear ho-

mogenous media, and can be generally explained by the Fresnel diffraction theory. In this Letter, to our knowledge for the first time, we demonstrate the nonlinear TE from propagating ABs and other rogue wave eigenmodes of the system that exhibit TE in a bulk NL medium.

Mathematical modeling.—The commonly used model to generate a soliton, a rogue wave, or a breather solution in one dimension is the scaled cubic NL Schrödinger equation (SE)

$$i\frac{\partial\psi}{\partial z} + \frac{1}{2}\frac{\partial^2\psi}{\partial x^2} + |\psi|^2\psi = 0. \quad (1)$$

A soliton solution is easily found by using the inverse scattering transform [18]. Among the rogue wave solutions of NLSE, AB was first reported by N. Akhmediev in 1980s [16]; it can be written as

$$\psi(z, x) = \frac{(1 - 4q) \cosh(az) + \sqrt{2q} \cos(\Omega x) + ia \sinh(az)}{\sqrt{2q} \cos(\Omega x) - \cosh(az)} \times \exp(iz), \quad (2)$$

where $q = (1 - \Omega^2/4)/2$ and $a = \sqrt{8q(1 - 2q)}$, with $q < 1/2$. The period of $\psi(z, x)$ along x is $D_x = \pi/\sqrt{1 - 2q}$. Specially, Eq. (2) will transform into

$$\psi(z, x) = \frac{\cos(\sqrt{2}x) + i\sqrt{2} \sinh(z)}{\cos(\sqrt{2}x) - \sqrt{2} \cosh(z)} \exp(iz), \quad (3)$$

when $q = 1/4$. If $q > 1/2$, the rogue wave solution of Eq. (1) is the KMB, which can be written as

$$\psi(z, x) = \frac{(1 - 4q) \cos(az) + \sqrt{2q} \cosh(\Omega x) - ia \sin(az)}{\sqrt{2q} \cosh(\Omega x) - \cos(az)} \times \exp(iz), \quad (4)$$

where now $q = (1 + \Omega^2/4)/2$ and $a = \sqrt{8q(2q - 1)}$. Different from AB, the KMB is periodic along the z axis,

with the period $D_z = \pi/\sqrt{2q(2q-1)}$. When $q = 1/2$, the solutions in Eqs. (2) and (4) degenerate into the fractional form

$$\psi(z, x) = \left[1 - \frac{4 + 8iz}{1 + 4x^2 + 4z^2} \right] \exp(iz), \quad (5)$$

which is known as the Peregrine soliton [13, 14]. In Fig. 1 we display three specific solutions of Eq. (1), corresponding to Eqs. (3), (5) and (4), respectively. It is seen that the AB transforms into the Peregrine soliton as q approaches $1/2$, which then transforms into the KMB as q further increases. The common characteristic of all breathers is that they ride on a small but finite background.

ABs are periodic along the transverse coordinate x , as exhibited in Fig. 1(a), so their intensity is infinite along the x axis. KMBs are periodic along the z axis, so they can be viewed as higher-order soliton solutions (the basic soliton solution being the hyperbolic secant function). One should bear in mind that the energy of KMB, as well as of the Peregrine soliton, is also infinite along the x axis. All these solutions are exact analytical solutions of the cubic NLSE. The question is, what happens when one propagates, as an input to Eq. (1), the solution which is not exactly the exact solution.

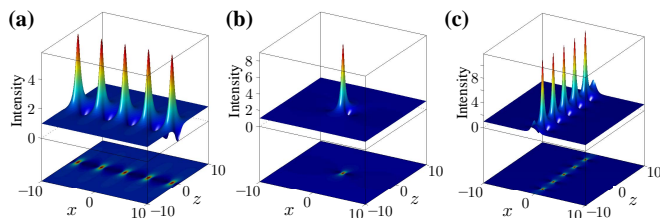


FIG. 1. (Color online) (a) AB with $q = 1/4$. (b) Peregrine soliton. (c) KMB with $q = 3/4$. Top panels present the intensity distributions, bottom panels the view from the above.

Numerical simulation and discussion.—Numerical simulations in this Letter are obtained by utilizing the fourth-order split-step fast Fourier transform (FFT) method [18] in double precision. To make beams of finite energy and prevent FFT spill-over effects, we utilize an aperture (filter) with a diameter large enough to enforce fast convergence of beam intensity to 0 when $|x| \rightarrow \infty$. Starting from Eq. (5), we construct an input to Eq. (1) with a finite energy of 2π , by using the profile subtracted from the uniform background in Eq. (5) at $z = 0$, $\psi_0(z = 0, x) = 4/(1 + 4x^2)$. The evolution of this profile is displayed in Fig. 2(a); it looks very much like a stable breather [19]. However, if one uses the whole transverse cross section of the Peregrine soliton at $z = 0$ as an input, which is the same as AB for $q = 1/2$, the evolution looks very different; it is shown in Fig. 2(b).

Curiously, instead of forming a breather or exhibiting a continuous diffraction in bulk media, the beam undergoes a “discrete” parabolic diffraction, quite similar to

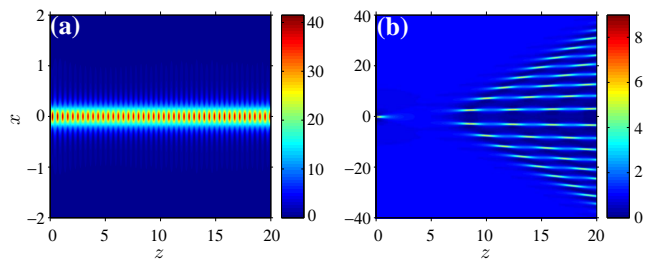


FIG. 2. (Color online) Propagation of ψ_0 (a) and Peregrine soliton (b).

the evolution of a discrete system [20]. It is also evident that the beam in each of the “channels” behaves like a breather during propagation. The explanation of the phenomenon is that actually the input wave is not an exact Peregrine soliton, but a slightly modulated wave, owing to the finite numerical accuracy at which the Peregrine profile is determined and to its finite energy. This modulated wave shows the tendency to diffract into an AB-like wave upon propagation. Thus, the cause of the phenomenon is the transverse modulational instability during the NL propagation.

We recall that there exists a more general Akhmediev solution of NLSE from Eq. (1), expressed in terms of Jacobi elliptic functions [16],

$$\psi(x, z) = k \frac{A(x) \operatorname{dn} \left(kz, \frac{1}{k} \right) + \frac{i}{k} \operatorname{sn} \left(kz, \frac{1}{k} \right)}{1 - A(x) \operatorname{cn} \left(kz, \frac{1}{k} \right)} \exp(iz), \quad (6)$$

in which

$$A(x) = \sqrt{\frac{1}{1+k}} \operatorname{cn} \left(\sqrt{2k}x, \sqrt{\frac{k-1}{2k}} \right)$$

with $k > 1$. When $k \rightarrow 1$, Eq. (6) reduces to Eq. (3). Because $\operatorname{sn}(x, m)$, $\operatorname{cn}(x, m)$ and $\operatorname{dn}(x, m)$ are all periodic and the corresponding periods are $4K$, $4K$ and $2K$ [21], respectively, with $K_m = \int_0^{\pi/2} d\theta / \sqrt{1 - m \sin^2 \theta}$, the solutions described by Eq. (6) are all periodic in both x and z directions. The corresponding periods can be deduced as

$$D_x = \frac{4}{\sqrt{2k}} K_{m=\sqrt{(k-1)/(2k)}} \text{ and } D_z = \frac{4}{k} K_{m=1/k},$$

respectively. Corresponding to Eq. (6) there exists another analytical solution of NLSE with $k < 1$ [16], but this eigenmode does not exhibit TE. The doubly-periodic Akhmediev solution from Eq. (6) does.

The intensity distribution of the solution with $k = 1.2$ is displayed in Fig. 3(a), with the result $D_x \approx 4.4$ and $D_z \approx 7.8$. It is clearly seen that the solution exhibits

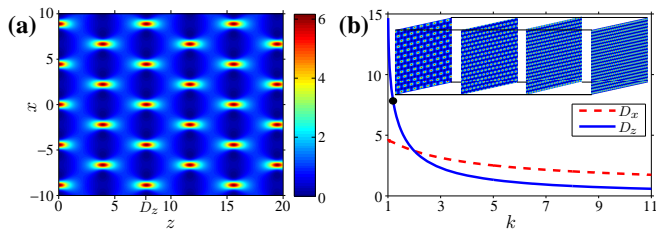


FIG. 3. (Color online) (a) Intensity of the solution in Eq. (6) for $k = 1.2$. (b) Periods D_x and D_z versus k . Insets show intensities of the solution with $k = 3, 5, 7$, and 9 , respectively. The dot on the D_z curve corresponds to (a).

the self-imaging TE-like property – the periodic incident wave exactly reappears at certain distances (an integer multiple of D_z) and its π -phase shifted image appears at the distances half-way in-between (an odd multiple of $D_z/2$). Thus, the self-imaging can be viewed as a TE with the TE length $z_T = D_z$. Different from the previous literature, such TE is completely nonlinear, because it originates from the eigenmodes of NLSE and propagates in a NL medium. In Fig. 3(b), we display the TE length z_T (viz., D_z), as well as the transverse period D_x of the solution, as functions of k ; they both monotonously decrease with increasing k .

To display the changing nonlinear TE with k more clearly, we show in the inset of Fig. 3(b) four special cases corresponding to $k = 3, 5, 7$ and 9 , respectively. When $k = 2$, $D_x = D_z$, and D_x and D_z will have a crossing point, as shown in Fig. 3(b). When $k \rightarrow 1$, $D_x \rightarrow \sqrt{2}\pi$ and $z_T \rightarrow +\infty$, as is visible in Fig. 3(b). Then, the solution indicated by Eq. (6) reduces to the AB solution described by Eq. (3) and illustrated by Fig. 1(a). Since Eq. (6) is an eigenmode solution of the NLSE in Eq. (1), the general AB can be viewed as the nonlinear TE eigenmode.

AB for $q = 1/4$ is a limiting case of the TE eigenmode. Therefore, we investigate evolution of the beam with the same profile as the AB at $z = 0$ plane, obtained at high but finite precision. Thus, we launch AB from Eq. (2) at $z = 0$ into the NL medium and follow its evolution; the result is shown in Fig. 4(a). It corresponds to the case given in Fig. 1(a) ($D_x = \sqrt{2}\pi$), evolving on a torus. It is clearly seen that AB displays the nonlinear TE during propagation. Owing to the modulational instability, it shows the tendency to diffract as the doubly-periodic Akhmediev solution from Fig. 3. In Fig. 4(b) the intensities of the beam during evolution are presented at the initial place ($z = 0$), half TE length ($z = z_T/2$), and the full TE length ($z = z_T$), respectively. The intensity distributions at z_T are the same as the launched ones, while those at $z_T/2$ display a π -phase shift. Thus, the NL Talbot carpet looks simple – only the primary and secondary images appear; the fractional images are absent. This may be a blessing in applications, because –

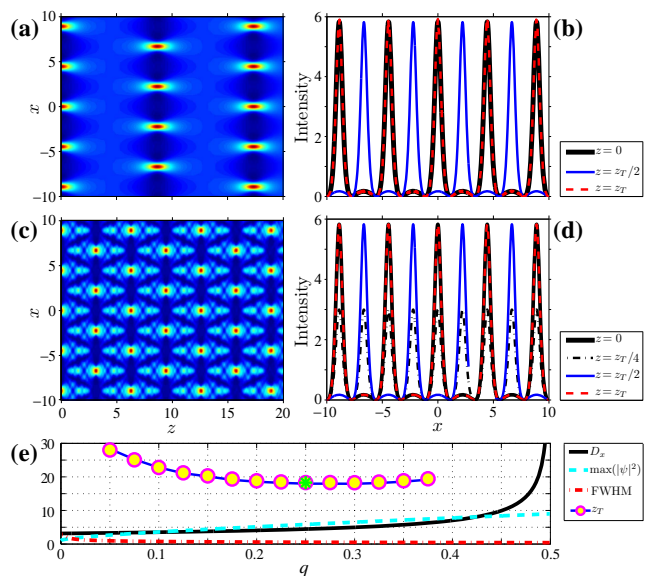


FIG. 4. (Color online) (a) NL TE carpet of the AB with $q = 1/4$. (b) Intensity profiles at certain distances. (c) and (d) Same as (a) and (b) but for the linear TE. (e) Spatial period D_x , the maximum intensity of the wave, FWHM of one peak intensity, and NL TE length z_T , all as functions of q . The star $*$ corresponds to (a).

e.g. for optical switching – fractional images are harmful.

To exemplify the difference between linear and nonlinear TE, we remove the NL term in Eq. (1) and follow the linear diffraction of the input AB; one obtains the evolution carpet shown in Fig. 4(c). This corresponds to the “NL TE” mentioned in Refs. [10, 11]. The usual Talbot carpet is revealed, displaying the fractional TE images as well [11]. Similar to Fig. 4(b), we exhibit the intensities of the linear TE at $z = 0$, $z = z_T/4$, $z = z_T/2$, and $z = z_T$ in Fig. 4(d). For the fractional linear TE at $z = z_T/4$, the period of the beam is halved, which is in accordance with the previous literature [3, 11]. In the linear case, the diffraction pattern (the input AB) undergoes the usual superposition and interference as it propagates. In the nonlinear case the superposition does not hold and the interference is strongly influenced by the diffractionless propagation of the input AB, which is an eigenmode of Eq. (1). The result is the NL TE.

Different from the TE of the eigenmode shown in Fig. 3, the TE here directly follows from the transversely periodic wave and it cannot be analytically explained by Eq. (6). Without an analytical expression for z_T in this case, we numerically estimate z_T for different q in Eq. (2); the results are shown in Fig. 4(e). Corresponding to Fig. 4(a), the value of z_T is approximately 18.3, as shown by the green star $*$ in Fig. 4(e). In the same figure we also exhibit the period D_x , the maximum intensity $\max\{|\psi|^2\}$, and the full width at half maximum (FWHM) of the peak intensity of AB versus q . It is seen that the TE length z_T first decreases and then increases

with q increasing. At the same time, D_x and $\max\{|\psi|^2\}$ monotonously increase with the increasing q , while the FWHM monotonously decreases. It is worth mentioning that when $q > 3/8$, the self-imaging at half TE length is becoming less perfect (not shown).

The NL TE effect in Fig. 4 can be understood as a result of the interaction – the NL interference – among the smooth breather lobes. With q increasing, the period D_x increases and the FWHM decreases, so that the interaction among the peaks weakens. Therefore, each peak tends to evolve in a manner similar to Fig. 2(b), which leads to the imaging getting worse and the TE getting diminished. When D_x is not too big, the interaction among the lobes results in the clearly visible TE. Phenomenologically, the change in z_T is in accordance with the changing trends of D_x and $\max\{|\psi|^2\}$. During interaction, D_x and $\max\{|\psi|^2\}$ can be viewed as a distance and a mass, according to the analogy with classical mechanics. The larger the mass and the shorter the distance, the stronger the interaction and the shorter the z_T . Thus, the interaction can be explained according to the behavior of $D_x/\max\{|\psi|^2\}$. When q is small, D_x is relatively big and $\max\{|\psi|^2\}$ is relatively small, thus z_T is large. With q increasing, the increase in D_x is smaller than that in $\max\{|\psi|^2\}$, so z_T decreases. However, when $q \rightarrow 1/2$, D_x increases fast and approaches $+\infty$, while $\max\{|\psi|^2\}$ tends to the maximum intensity of Eq. (5); therefore z_T starts to increase again.

Conclusion.—We have demonstrated the NL TE in the cubic NL medium, coming from ABs and other rogue waves. It is a genuine NL optical effect, arising from the transverse modulational instability and the NL interference of AB lobes. Its defining feature is the presence of only primary and secondary images; no fractional images are seen. We have shown that the TE length of the NL TE is determined by the intensity and the period of ABs. Owing to the simple Talbot carpet, the NL TE can find potential applications in all-optical communications.

This work was supported by the 973 Program (2012CB921804), NSFC (61308015), CPSF (2012M521773), and NPRP 09-462-1-074 project from the Qatar National Research Fund (a member of the Qatar Foundation). The NSFC (61078002, 61078020, 11104214, 61108017, 11104216, 61205112) projects are also acknowledged.

* zhangyiqi@mail.xjtu.edu.cn

† milivoj.belic@qatar.tamu.edu

‡ ypzhang@mail.xjtu.edu.cn

[1] H. F. Talbot, *Philos. Mag.* **9**, 401 (1836).

- [2] L. Rayleigh, *Philos. Mag.* **11**, 196 (1881).
- [3] J. Wen, S. Du, H. Chen, and M. Xiao, *Appl. Phys. Lett.* **98**, 081108 (2011); Y. Q. Zhang, X. Yao, C. Z. Yuan, P. Y. Li, J. M. Yuan, W. K. Feng, S. Q. Jia, and Y. P. Zhang, *IEEE Photon. J.* **4**, 2057 (2012).
- [4] X.-B. Song, H.-B. Wang, J. Xiong, K. Wang, X. Zhang, K.-H. Luo, and L.-A. Wu, *Phys. Rev. Lett.* **107**, 033902 (2011).
- [5] R. Iwanow, D. A. May-Arrijoja, D. N. Christodoulides, G. I. Stegeman, Y. Min, and W. Sohler, *Phys. Rev. Lett.* **95**, 053902 (2005).
- [6] H. Ramezani, D. N. Christodoulides, V. Kovanis, I. Vitebskiy, and T. Kottos, *Phys. Rev. Lett.* **109**, 033902 (2012).
- [7] L. Deng, E. W. Hagley, J. Denschlag, J. E. Simsarian, M. Edwards, C. W. Clark, K. Helmerson, S. L. Rolston, and W. D. Phillips, *Phys. Rev. Lett.* **83**, 5407 (1999); C. Ryu, M. F. Andersen, A. Vaziri, M. B. d’Arcy, J. M. Grossman, K. Helmerson, and W. D. Phillips, *ibid.* **96**, 160403 (2006).
- [8] F. Pfeiffer, M. Bech, O. Bunk, P. Kraft, E. F. Eikenberry, C. Brönnimann, C. Grünzweig, and C. David, *Nature Mater.* **7**, 134 (2008).
- [9] B. Brezger, L. Hackermüller, S. Uttenthaler, J. Petschinka, M. Arndt, and A. Zeilinger, *Phys. Rev. Lett.* **88**, 100404 (2002).
- [10] Y. Zhang, J. Wen, S. N. Zhu, and M. Xiao, *Phys. Rev. Lett.* **104**, 183901 (2010).
- [11] J. Wen, Y. Zhang, and M. Xiao, *Adv. Opt. Photon.* **5**, 83 (2013).
- [12] D. R. Solli, C. Ropers, P. Koonath, and B. Jalali, *Nature* **450**, 1054 (2007); A. Montina, U. Bortolozzo, S. Residori, and F. T. Arecchi, *Phys. Rev. Lett.* **103**, 173901 (2009); S. Birkholz, E. T. J. Nibbering, C. Brée, S. Skupin, A. Demircan, G. Genty, and G. Steinmeyer, *ibid.* **111**, 243903 (2013); W.-P. Zhong, M. R. Belić, and T. Huang, *Phys. Rev. E* **87**, 065201 (2013).
- [13] B. Kibler, J. Fatome, C. Finot, G. Millot, F. Dias, G. Genty, N. Akhmediev, and J. M. Dudley, *Nature Phys.* **6**, 790 (2010).
- [14] D. H. Peregrine, *J. Aust. Math. Soc. Ser. B* **25**, 16 (1983).
- [15] Y.-C. Ma, *Stud. Appl. Math.* **60**, 43 (1979); B. Kibler, J. Fatome, C. Finot, G. Millot, G. Genty, B. Wetzel, N. Akhmediev, F. Dias, and J. M. Dudley, *Sci. Rep.* **2**, 463 (2012).
- [16] N. Akhmediev, V. Eleonskii, and N. Kulagin, *Theor. Math. Phys.* **72**, 809 (1987).
- [17] M. Erkintalo, K. Hammani, B. Kibler, C. Finot, N. Akhmediev, J. M. Dudley, and G. Genty, *Phys. Rev. Lett.* **107**, 253901 (2011); D. J. Kedziora, A. Ankiewicz, and N. Akhmediev, *Phys. Rev. E* **88**, 013207 (2013).
- [18] J. Yang, *Nonlinear Waves in Integrable and Non-Integrable Systems* (SIAM, Philadelphia, 2010).
- [19] J. Satsuma and N. Yajima, *Prog. Theor. Phys. Supplement* **55**, 284 (1974).
- [20] F. Lederer, G. I. Stegeman, D. N. Christodoulides, G. Asanto, M. Segev, and Y. Silberberg, *Phys. Rep.* **463**, 1 (2008); I. L. Garanovich, S. Longhi, A. A. Sukhorukov, and Y. S. Kivshar, *ibid.* **518**, 1 (2012).
- [21] M. Abramowitz and I. A. Stegun, *Handbook of Mathematical Functions* (Dover Publications Inc., 1970).